RICE UNIVERSITY

Comparison of estimates of airmass aging

using particle and other measurements near Fort Worth, TX

by

Basak Karakurt Cevik

A THESIS SUBMITTED

IN PARTIAL FULFILLMENT OF THE

REQUIREMENTS FOR THE DEGREE

Master of Science

APPROVED, THESIS COMMITTEE:

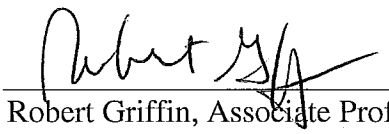

Robert Griffin, Associate Professor of Civil and Environmental Engineering, Rice University

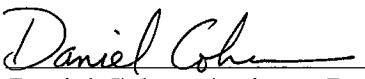

Daniel Cohan, Assistant Professor of Civil and Environmental Engineering, Rice University

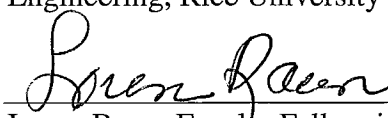

Loren Raun, Faculty Fellow in Statistics, Rice University

Houston, TX

2012

RICE UNIVERSITY

Comparison of estimates of airmass aging

using particle and other measurements near Fort Worth, TX

by

Basak Karakurt Cevik

A THESIS SUBMITTED

IN PARTIAL FULFILLMENT OF THE

REQUIREMENTS FOR THE DEGREE

Master of Science

APPROVED, THESIS COMMITTEE:

Robert Griffin, Associate Professor of Civil and Environmental Engineering, Rice University

Daniel Cohan, Assistant Professor of Civil and Environmental Engineering, Rice University

Loren Raun, Faculty Fellow in Statistics, Rice University

Houston, TX

2012

ABSTRACT

Comparison of estimates of airmass aging

using particle and other measurements near Fort Worth, TX

by

Basak Karakurt Cevik

The composition, concentration, and size of submicron aerosols were measured with a time resolution of five minutes by an Aerodyne high-resolution time-of-flight aerosol mass spectrometer (HR-ToF-AMS) at a rural location northwest of the Dallas-Fort Worth, TX, area for the month of June 2011. A TSI, Inc., Model AE51 aethalometer using an optical absorption technique also was deployed to measure black carbon (BC) concentrations. The total measured PM_1 mass concentration ranged between 1.0 $\mu g/m^3$ and 17.1 $\mu g/m^3$, with a mean and standard deviation of 4.6± 2.7 $\mu g/m^3$. Significant variability is observed in the time series of total PM_1 and of all four HR-ToF-AMS species, particularly between June 21 and 25. The average aerosol composition was dominated by organic matter (52.1 ± 14.8%) and sulfate (28.8 ± 11.8%). Organic aerosol concentrations were positively correlated with tracers of combustion carbon monoxide (CO) and BC, the coefficients of determination were r^2=064 and r^2=0.48, respectively.

Because of the large influence of organics on total aerosol concentration, organic data were analyzed in the context of ΔOA/ΔCO, which typically is used to investigate the relative importance of secondary organic aerosol. The average ΔOA/ΔCO for the data used was 64.0 ± 26.9 μg/ (m^3 ppmv), which is typical of an aged air mass. Other metrics of age include the ratio of OOAI (more oxidized) to total oxidized organic aerosol (OOA), the ratio of sulfate to total sulfur, the ratio of its oxidation products to isoprene, and the ratio of nitrogen oxides to total reactive nitrogen. All metrics point to aged air masses, but variations in these age matrices, particularly during one period of enhanced ΔOA/ΔCO, help elucidate the contributions of various precursors and processes to organic aerosols at the site.

ACKNOWLEDGEMENTS

First and foremost, I would like to thank my advisor Dr. Robert Griffin for his patience and guidance during my study; this study would not have been possible without his support. I am also grateful to our former post-doc, Dr. Andrew P. Rutter, for training me in lab, being willing to help me anytime I needed it, and providing PMF data. I also would like to thank Dr. Barry Lefer and James Flynn for providing CO and meteorological data and Dr. Saewung Kim for providing VOC data. Lastly, I would like to express my special gratitude and thanks to my friends Kabindra Shakya, Owen Gong, and Caroline Gutierrez with whom I worked in the field.

TABLE OF CONTENTS

List of Figures

List of Tables

CHAPTER 1

INTRODUCTION

Aerosols or particulate matter (PM) are solid or liquid particles suspended in air. They are generally assumed to be spherical, and their size ranges from a few nanometers (nm) to tens of micrometers (μm) in diameter. Particles directly emitted into the atmosphere from natural or anthropogenic sources are referred to as primary aerosols, and the particles that are formed in the atmosphere through the oxidation of precursor gases, such as sulfur dioxide (SO_2), nitrogen oxides (NO_x = nitric oxide (NO) plus nitrogen dioxide (NO_2)), and volatile organic compounds (VOCs), are referred to as secondary aerosol.

Atmospheric aerosol concentrations may result from a wide variety of natural and anthropogenic sources. The natural sources of aerosols include wind-driven soil dust, volcanic eruptions, sea salt, biological debris and extraterrestrial dust, whereas biomass burning, fossil fuel combustion, industrial processes, and construction works are examples of anthropogenic sources (Seinfeld and Pandis, 2006). Most PM have relatively short lifetimes in the troposphere (a few days to a few weeks) and are removed from the atmosphere by dry and wet deposition before they reach the stratosphere. As such, the only source of aerosols that causes direct injection into the stratosphere is volcanic eruption.

The size of the particle is an important factor that determines its removal mechanism, transformation, optical properties, and health effects. Particulate matter is divided in to two main modes based on size: fine particles with a diameter 2.5 μm and smaller and coarse particles with a diameter larger than 2.5 μm. Fine particles consist of two sub-modes: nucleation and accumulation. Nucleation mode particles have a diameter up to 100 nm, and they dominate the total aerosol number concentration. These particles are formed by homogenous nucleation or condensation of hot vapor during combustion processes. They form larger particles by coagulation. The accumulation range includes the particles with a diameter between 0.1 to 2.5 μm and dominates the total aerosol surface area. The particles in this range are formed by coagulation of nucleation particles or condensation of vapor onto existing aerosol. Accumulation mode particles have relatively long lifetimes. Coarse particles include windblown dust, sea salts, volcanic emissions, plant particles, and mechanically generated anthropogenic particles. These particles are removed from the atmosphere easily by sedimentation because of their relatively large size.

Aerosols have important impacts on climate, visibility, and public health. Aerosols affect Earth's climate directly by scattering (cooling effect) or absorbing (warming effect) sunlight. In addition, particles serve as condensation nuclei for cloud droplet formation. Increased concentrations of aerosols that act as cloud condensation nuclei increase the total droplet concentration and as a result increase the albedo (brightness) of clouds and decrease the size of the water droplets in the clouds. The decrease in water droplet size results in increased cloud lifetime. Certain types of aerosols also may trigger ice formation and activate cold cloud formation (Saunders et

al., 2010; Hoose and Mohler, 2012). Ice nucleation also drives radiative forcing. Such cloud effects are considered an indirect climate effect of particles.

The impact of aerosols on visibility is caused mainly by the scattering of visible light by particles between 0.1 and 1.5 μm in diameter. Essentially such particles prevent light reflected by objects from reaching the eye of the viewer. In addition, sunlight scattered by particles results in a background haze that also contributes to visibility reduction (Pöschl, 2005).

The concentrations of aerosols in the troposphere play an important role in human health, as increased levels of PM have been correlated strongly to increased rates of human respiratory and allergic illnesses and death (Pope et al., 2002). This is especially important for ultrafine particles (diameter smaller than 100 nm) that are speculated to have adverse effects on human health because they are small enough to penetrate deeper into lungs, enter the blood stream, and be transported to the nerves in the brain (Nemmar et al., 2001). Moreover, toxicological studies show that ultrafine particles have considerably elevated toxicity per unit mass (Donaldson and MacNee, 1998). For both ultrafine and coarse aerosols, physical and chemical characteristics determine their adverse health effects (Pöschl, 2005).

Recent ozone (O_3) levels in the atmosphere of the Dallas-Fort Worth (DFW) region have exceeded the National Ambient Air Quality Standards established by the Environmental Protection Agency. While O_3 is produced naturally to some extent in the atmosphere, NO_x and VOCs are the main precursors that lead to excessive O_3 formation in polluted tropospheric areas. Since the DFW area does not have large petrochemical

facilities, the most important anthropogenic emission sources of NO_x and VOCs in the area appear to be motor vehicles and large point sources such as electric power plants and cement kilns. Despite the decreases in the NO_x and VOC emissions from automobiles, O_3 levels in the DFW area have not decreased as significantly as would be expected in recent years. It is speculated that the O_3 levels in the region are affected by the increase in the number of natural gas wells and the production of natural gas in the DFW area. To investigate these relatively high O_3 levels in the DFW area, a temporary ground-based photochemical "supersite" was established at the Eagle Mountain Lake (EML) Texas Commission on Environmental Quality (TCEQ) monitoring site during June 2011. While the primary focus of the field campaign was to investigate O_3 formation routes and rates, considerable effort also was made to characterize quantitatively the sub-micron PM simultaneously. This thesis describes these efforts with a focus on determination of whether the observed PM was formed in situ or transported upwind through investigation of air mass aging.

CHAPTER 2

MATERIAL and METHODS

Site Description and Meteorology

Measurements were performed continuously in June 2011 at the EML TCEQ monitoring site, which is located 226 m above sea level, in Fort Worth, TX, at 32° 59'16" N, 97° 28' 37" W (Figure 1a). The site is in a semi-rural area and is ~40 km northwest of downtown Fort Worth. The DFW area is the largest metropolitan in Texas and the fourth largest metropolitan area in the United States, with a population of approximately 6.5 million people. The site is flat and includes various grasses and shrubs (Figure 1b). It is located a few kilometers west of a minor state highway near several natural gas operations. The land on which the site sits is owned by the United States National Guard and is used as rangeland for cattle.

During the campaign, the wind speed and direction were fairly stable. The average wind speed was 7.9 m s^{-1}, and the wind direction was almost continuously southerly and southeasterly throughout the campaign, which placed the site downwind of the DFW metropolitan area. There was thunderstorm activity during the night of June 21, which was the only time during the campaign with measureable precipitation. The temperature varied from 17.7 to 39.6 ºC, and the relative humidity ranged from 13.8% to 93.3% during the sampling time. Temperature and relative humidity all varied diurnally. Days were generally cloud-free.

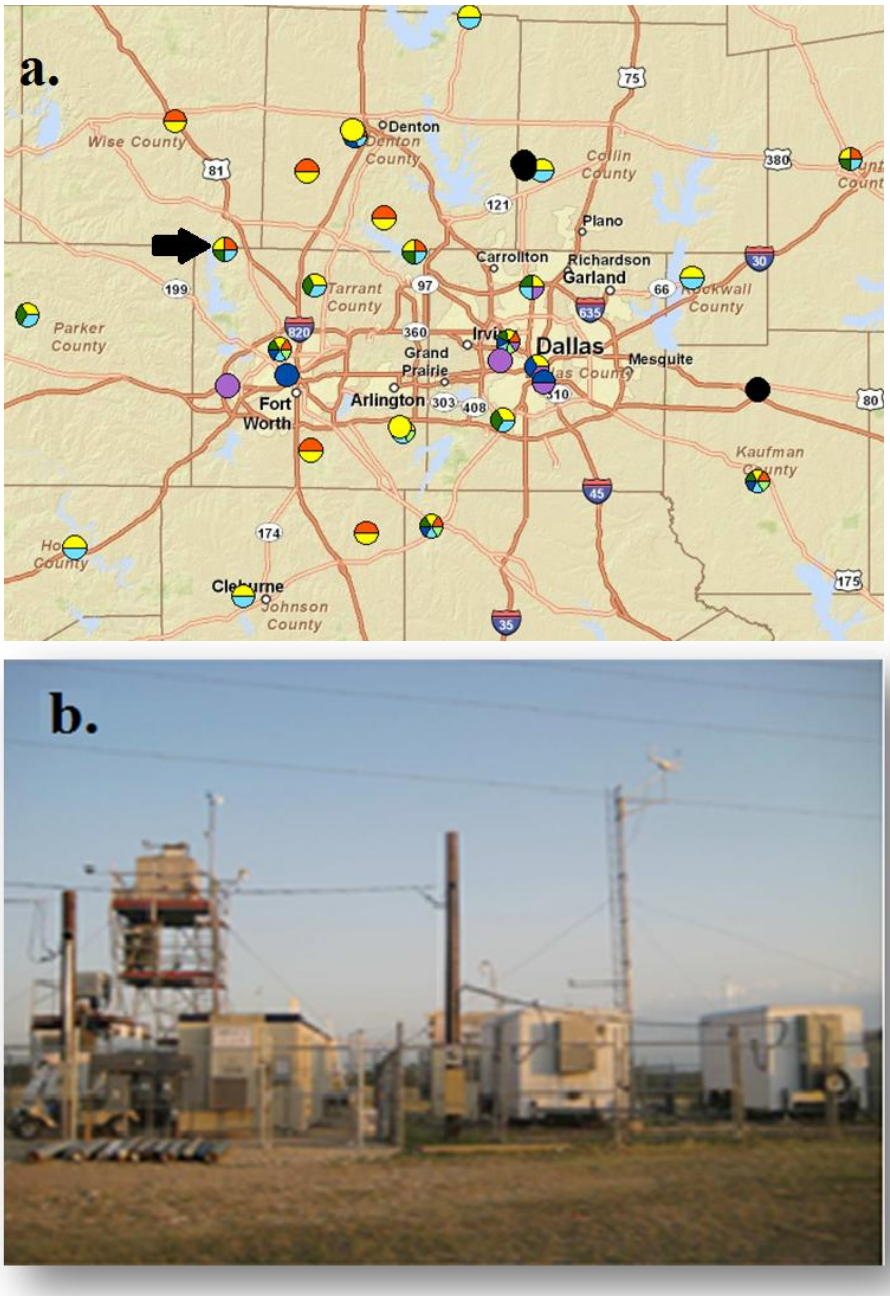

Figure 1 a.) Map indicating the location of the EML site (black arrow) relative to the DFW metropolitan area. b.) Photograph of the sampling site at EML. The instrument trailer is shown to the left. Two existing TCEQ trailers are shown to the right.

Particle Instrumentation

Particles were sampled from a main copper tubing inlet. An Aerodyne high-resolution time-of-flight aerosol mass spectrometer (HR-ToF-AMS), a Brechtel Manufacturing, Inc. particle-into-liquid sampler (PILS) connected to Dionex ion chromatographs (IC), and a TSI, Inc. Model AE51 aethalometer subsampled from the main inlet, which was equipped with a 2.5-µm cyclone.

The HR-ToF-AMS is an online measurement of size-resolved chemistry of submicron atmospheric aerosol. It provides real time data with high time resolution and high sensitivity. The description of the instrument is given in detail elsewhere (DeCarlo et al., 2006) so only a brief description is included here. Air is sampled through a critical orifice and enters an aerodynamic lens, which forces particles to focus into a narrow beam, which is then accelerated into a vacuum chamber. The size of the particle is measured by the flight time of the particle through this region (the PToF). The entrance time for particle flight is determined by a rotating chopper; the time to traverse the PToF region is determined by detection of particle material by the mass spectrometer. With a known distance and these times, a velocity is determined, with velocity inversely proportional to the particle vacuum aerodynamic diameter. After the particles pass through the PToF region, they are vaporized after impacting on a heated surface (600 ºC) and then ionized by electron impact. The resultant ions are detected by a time-of-flight

mass spectrometer and attributed to specific aerosol species based on their mass/charge ratios. The HR-ToF-AMS can detect sulfate, nitrate, ammonium, chloride, and organic species (DeCarlo et al., 2006). The lower detection limit for the instrument was below 200 ng/m^3 for all five species, and the estimated uncertainty was ±25%.

The PILS provides an online measurement of water-soluble ionic aerosol chemical composition at a resolution of 16 minutes. The PILS collects particles on an impaction surface by growing them through exposure to a saturated steam environment. A solution containing aerosol species for injection to the ICs (Dionex ICS 1600) is generated by washing the impaction surface with deionized water (Weber et al. 2001; Orsini et al. 2003). Sulfate ion concentrations measured with the PILS-ICs are used to determine the collection efficiency of the HR-ToF-AMS. (All data shown have been corrected for this efficiency.) The instrument detection limit for sulfate was 0.15 μg/m^3.

The TSI, Inc. Model AE51 aethalometer quantifies black carbon (BC) concentration every three minutes by measuring the attenuation of a light beam transmitted through particles that are continuously collected on a filter. The filter was changed once per day. The measurement uncertainty and detection limit were both 0.001 μg/m^3.

The HR-ToF-AMS was calibrated for ionization efficiency, particle sizing, and inlet flow every two weeks. The PILS and AE51 inlet flows were calibrated at the start of campaign. The ICs were calibrated once per week with six-point standard curves using seven anion and six cation standard mixed solutions obtained from Dionex Corporation. Because of particle contamination caused by an oil-based pump being used

by another research group at the EML TCEQ site, only data from June 17 through the end of the campaign are presented here. Other gaps in the data presented result from calibration, instrument maintenance, or other similar issues.

Additional Measurements

Additional measurements made at the site and used in this analysis include mixing ratios of trace gases including carbon monoxide (CO), NO_2, NO, total active nitrogen (NO_y), SO_2, and VOCs; meteorological data also were tracked. A Thermo Scientific CO Analyzer (Model 48C-Trace Level Enhance (TLE)) quantifies CO with a gas correlation wheel cell that detects CO via the absorption of infrared radiation at a wavelength of 4.6 micron. The principle of the Thermo Scientific Model 42 trace level chemiluminescence NO-NO_2-NO_x analyzers is based on the fact that NO and O_3 react to produce light of a characteristic wavelength, with an intensity linearly proportional to the NO concentration. The Thermo Scientific Model 43i-TLE SO_2 instrument determines the concentration of SO_2 by measuring the emitted fluorescence of SO_2 produced by the absorption of ultraviolet light. A Proton Transfer Reaction – Mass Spectrometer (PTR-MS) allows for real-time measurements of VOCs. In the PTR-MS, the air to be analyzed is pumped continuously through a drift tube reactor, and a fraction of the VOCs is ionized in proton-transfer reactions with hydronium ions (H_3O^+). The resulting cation is detected and quantified by a quadrupole mass spectrometer.

Analytical Methods

PMF Analysis

Positive matrix factorization (PMF) modeling was performed on the HR-ToF-AMS data to separate the main components of the total organic aerosol (Lanz et al. 2007; Ulbrich et al. 2009). PMF uses a mass balance analysis on each mass spectrum measured to apportion total organic aerosol into a number of factors. That is, the model determines for a given number of factors, how spectra representing each factor be combined to minimize the difference between the observed and modeled overall mass spectrum. When performed for each spectrum collected, the model provides a time series of each factor's contribution to the overall organic aerosol concentration. The model does not require a priori information about factor profiles, and the number of factors used was determined during the minimization of residuals procedure. The model identified three factors: one with a mass spectrum dominated by $C_3H_5^+$ (m/z 41) with a contribution of 0.6% and $C_3H_7^+$ (m/z 43) with a contribution of 0.6% to total organic aerosol (termed hydrocarbon-like organic aerosol (HOA)), one dominated by CO_2^+ (m/z 44), and a third with no contribution from the HOA fragments but decreased relative importance of m/z 44 (Lanz et al. 2007). These last two categories are termed oxidized organic aerosol (OOA). More specifically, the OOA with the larger relative levels of m/z 44 is termed OOAI and is thought to be OOA that has experienced more extensive oxidation. Contribution of m/z 44 to each OOA is 30% and 16% to total organic aerosol, respectively. Detailed spectra appear in Rutter et al. (in preparation).

ΔOA/ΔCO Analysis

Analysis of the ratio of organic aerosol (OA) to CO has been used previously to investigate the aging and formation of secondary organic aerosols (SOA) (de Gouw et al. 2005; Cottrell et al. 2008; Kleinman et al. 2008; DeCarlo et al. 2010). Carbon monoxide is a fairly conservative pollutant due to a lifetime with respect to hydroxyl radical oxidation that is on the order of two months. Therefore, any dilution effect on the time scale of hours to days can be minimized by analyzing the ratio of OA to CO (Hodzic and Jimenez, 2011). Because CO and primary organic aerosols generally have similar emission sources, their concentration ratios are expected to be somewhat constant in the source region over a short timeframe (de Gouw et al. 2009; Hodzic and Jimenez, 2011). Consequently, any increases in the ratio of ΔOA (measured OA minus background OA) to ΔCO (measured CO minus background CO) can be used as an indicator of SOA formation.

To calculate the ΔOA/ΔCO ratio, the fifth percentiles of CO mixing ratio and OA concentrations are used as background levels (82.9 ppb and 0.6 $\mu g/m^3$, respectively) and subtracted from measured values in this study. The OA concentration and the CO mixing ratios that were smaller than 1.5 times the calculated respective background values are excluded (Cottrell et al. 2008).

Airmass Age Indices

Different photochemical age surrogates were used to evaluate the age of the air mass in the DFW area. The age of the observed air masses with respect to SO_2 is calculated by the ratio of sulfate to total sulfur (assuming sulfate and SO_2 constitute total

sulfur), $SO_4^{2-}/(SO_4^{2-}+SO_2)$, because emitted SO_2 in the source region is oxidized to sulfuric acid (Quinn, et al. 2005). The photochemical age is expected to increase with the increase in the ratio of $SO_4^{2-}/(SO_4^{2-}+SO_2)$ since SO_4^{2-} formation from emitted SO_2 will require photochemical processing. Because sulfur is predominantly emitted from coal-burning power plants, this aging metric is similar to plume age. The age of the air mass with respect to NO_x is approximated with the value of $-\log (NO_x/NO_y)$. NO_x, which is emitted mostly by fossil fuel combustion, is oxidized to species like nitric acid (HNO_3), nitrous acid(HONO), nitrate radical (NO_3), dinitrogen pentoxide (N_2O_5), peroxynitric acid (HNO_4), and peroxyacetylnitrate (PAN) as the air photochemically processed. Since NO_y includes both NO_x and all of its oxidation products, photochemical age increases with the increase of $-\log (NO_x/NO_y)$ ratios, and smaller values represent fresh emissions with not enough time to processed in to NO_y (Kleinman et al. 2007; DeCarlo et al. 2008; Slowik, et al. 2011). This metric represents aging with respect to a combusion source. The mixing ratios of isoprene oxidation products methacrolein (MACR) and methyl-vinylketone (MVK) to the mixing ratio of isoprene is used as an indicator of aging with respect to biogenic VOCs (de Gouw, et al. 2005; Cottrell, et al. 2008). As above, larger ratios of (MACR+MVK)/isoprene indicate more aged air and smaller ratios indicate fresh biogenic emissions. Lastly, the ratio of OOAI to total OOA OOAI/(OOAI+OOAII) is used to approximate the air mass aging with respect to VOC or aerosol-phase oxidation. Because OOAI is less volatile and more oxidized than OOAII (based on m/z 44), it is presumed that older air will have a larger relative contribution of OOAI because of the increased opportunity for oxidation.

It is important to note that these ratios are only approximations of the air mass aging because the calculation of the real age is more complicated, requires reaction rates and oxidant levels, and depends on atmospheric conditions. However, it should be noted that all metrics are expected to increase with air mass aging. In addition, it is hypothesized that relationships between $\Delta OA/\Delta CO$ and any of these age metrics may allow insight into potential SOA sources.

CHAPTER 3

RESULTS AND DISCUSSION

PM_1 chemical composition

The time series of organics, sulfate, nitrate, and ammonium mass concentrations measured with HR-ToF-AMS and the BC mass concentration measured with the AE51 and the total PM_1 concentration (sum of these species) is shown in Figure 2a. Chloride mass concentrations are not included because concentration was below or very close to the instrument detection limit most of the time. The total PM_1 mass concentration ranged between 1.0 $\mu g/m^3$ and 17.1 $\mu g/m^3$, with a mean of 4.9 $\mu g/m^3$. Significant variability is observed in the time series of total PM_1 and for all four species. Large spikes in concentrations are observed particularly between June 21 and 25. Except the spikes at midnight on June 24 and 25, the large spikes are driven by increases in the organics.

The average aerosol composition was dominated by organic matter (52.1 ± 14.8%) and sulfate (28.8 ± 11.8%), followed by smaller contributions from ammonium (10.0 ± 3.7%), nitrate (2.9 ± 1.4%), and BC (6.2 ±5.8%). The most abundant species was usually organics, with a few exceptions of sulfate mass concentrations exceeding organics (Figure 2b).

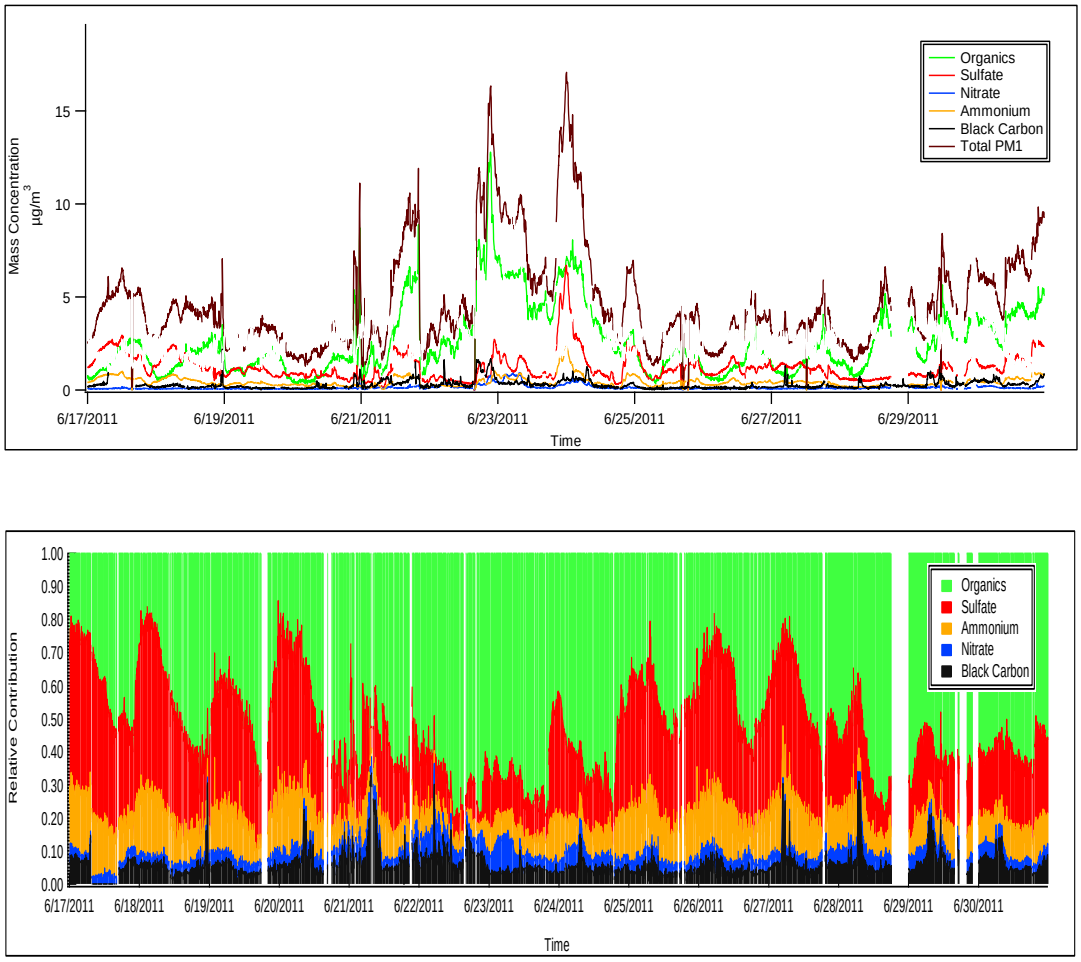

Figure 2 a.) Time series of mass concentrations (µg/m^3) of organic matter, sulfate, ammonium, and nitrate measured with HR-ToF- AMS and BC measured with the AE51. b.) The time series of the relative contribution of each chemical species to measured PM_1.

The average organic aerosol concentration was 2.6 ± 1.9 µg/m^3 with a wide range of 0.2 to 12.8 µg/m^3. Organic aerosol was positively correlated with anthropogenic tracers such as CO and BC indicating a relationship between organic aerosol and combustion activities . The coefficients of determination are r^2=0.64 and r^2=0.47. respectively. HOA, more oxidized (OOA I) and less oxidized (OOA II) secondary OA materials, accounted for 17.9±13.3%, 24.7±15.0% and 57.4±22.87% respectively, of the

observed OA mass. The HOA component was positively correlated well with BC and CO and the coefficients of determinations were r^2 0.62 and 0.44, respectively). OOA-II correlates with CO (r^2 = 0.61) which indicates it is mostly dominated by relatively fresh urban SOA. OOA II also positively correlated with nitrate aerosol quite well ($r^{2=}$0.60).

Over the campaign, the average sulfate mass concentration was 1.3 ± 0.7 μg/m^3, with a range of 1.2 to 6.6 μg/m^3. The rapid increase in the sulfate concentration on the night of June 24 is also observed in SO_2 mixing ratios and particle number concentrations. The average ammonium concentration was 0.6 ± 0.3 μg/m^3, with a range between 0.9 and 2.9 μg/m^3. The time series of ammonium and sulfate are well correlated (r^2 = 0.88), indicating the predominance of ammonium sulfate relative to ammonium nitrate. This is expected due to the high temperatures during the sampling period. Nitrate concentrations show correlation (r^2 = 0.54) with organic matter, which may indicate similar volatility.

As shown in Figure 3, a slight increase is observed in the organic matter diurnal profile during the afternoon as a result of photochemical production. The BC concentration profile during the day shows peak concentrations during rush hours, as expected. While no significant diurnal pattern is observed for the inorganic aerosol species, their concentrations show much more variability overnight. For sulfate, this is mirrored in the SO_2 diurnal profile (not shown). Ammonium diurnal behavior is then likely driven by that of sulfate. Small decreases in temperature overnight may have lead to the small variation in nitrate concentrations at night. As expected with environmental data, all boxplots of the data indicate a left skewed distributional shape.

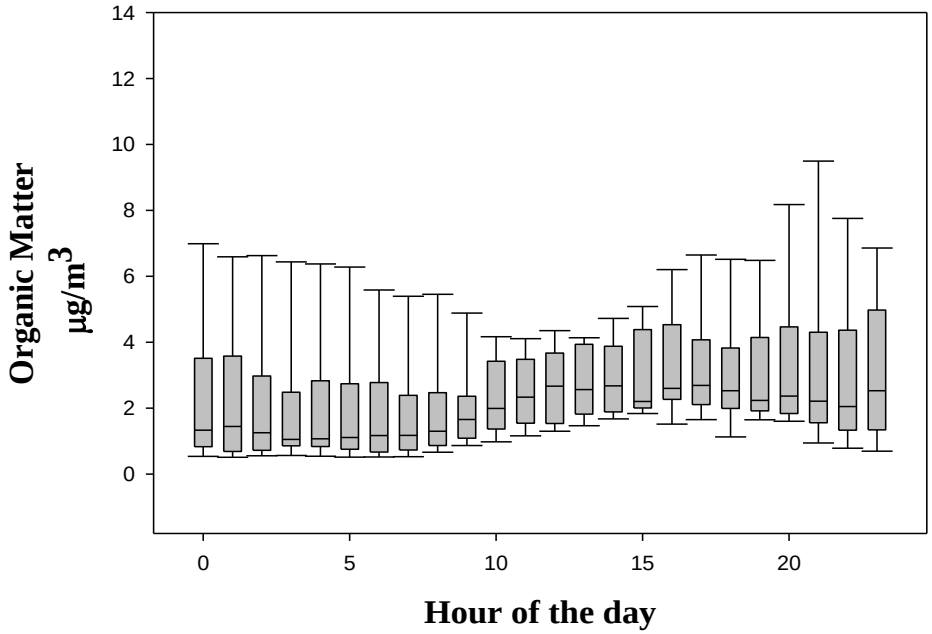
Organic Matter
µg/m3
14
12
10
8
6
4
2
0
0
5
10
15
20
Hour of the day

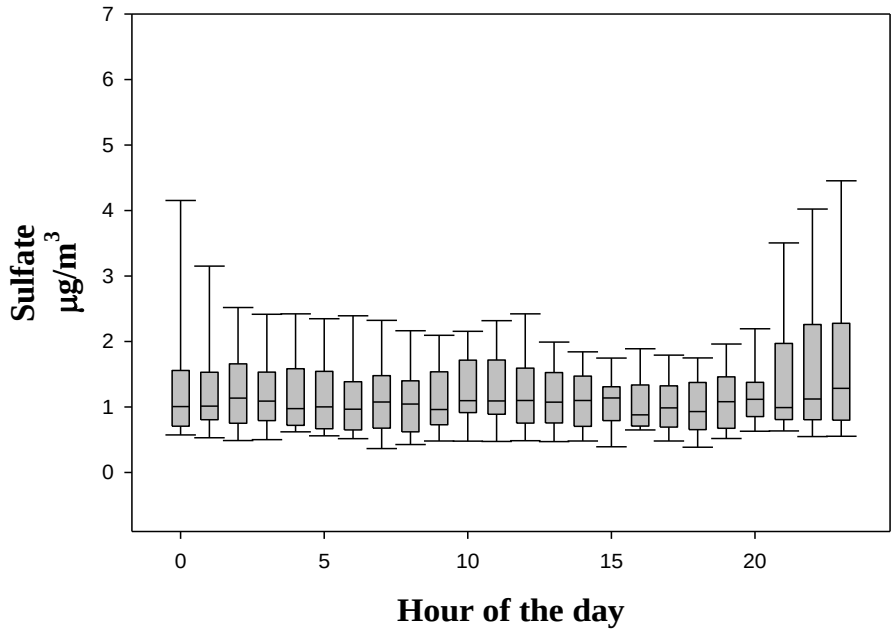
Sulfate
µg/m3
7
6
5
4
3
2
1
0
0
5
10
15
20
Hour of the day

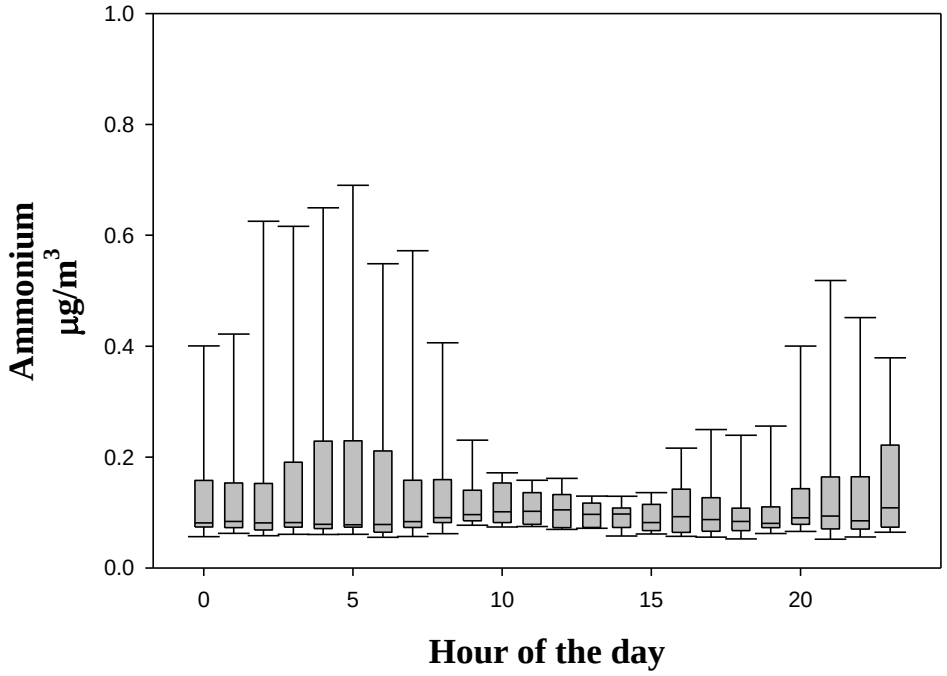
Ammonium
µg/m3
1.0
0.8
0.6
0.4
0.2
0.0
0
5
10
15
20
Hour of the day

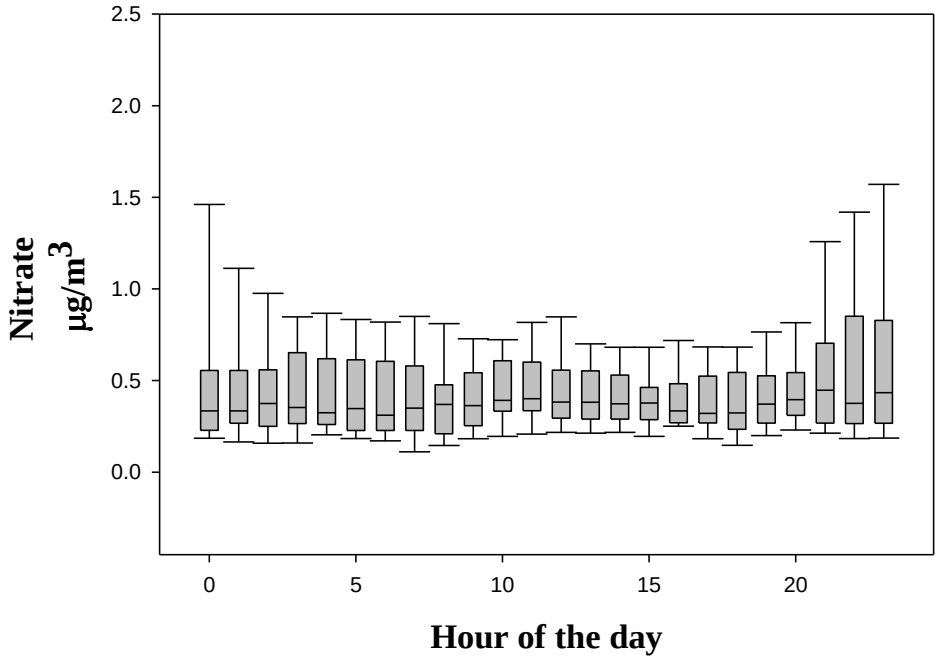
Nitrate
µg/m3
2.5
2.0
1.5
1.0
0.5
0.0
0
5
10
15
20
Hour of the day

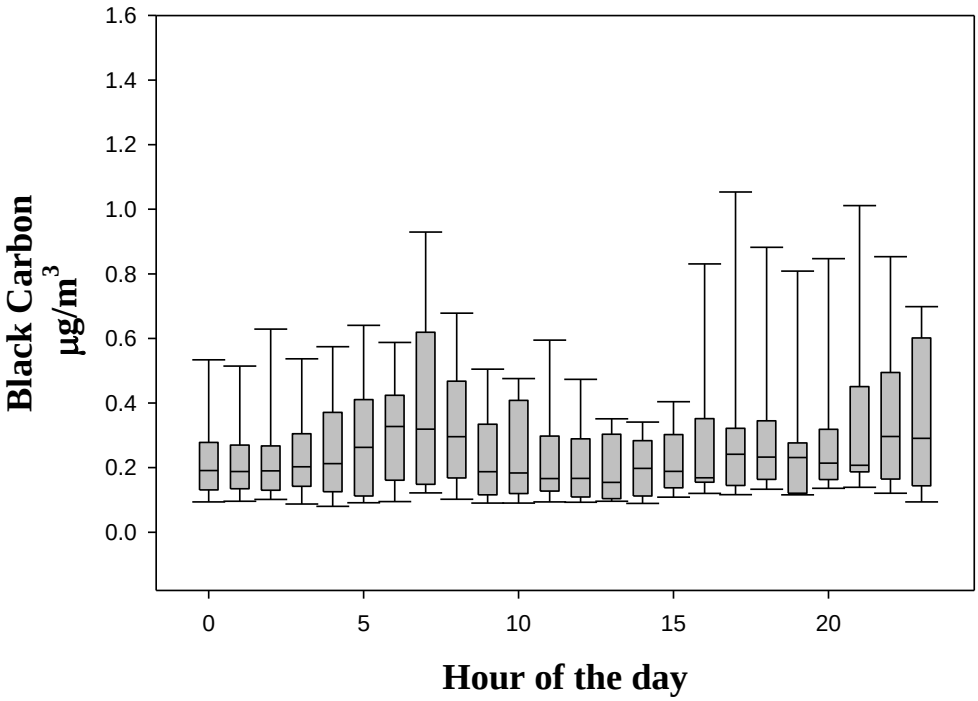

Figure 3. Diurnal profile box plots of PM_1 species. The band in the middle shows the median, and the bottom and the top of the boxes represent the 25 and 75 percentiles. The ends of the whiskers represent 5 and 95 percentiles.

ΔOA/ΔCO Analysis

The ΔOA/ΔCO ratios are calculated as µg/m^{3}ppmv. The average ΔOA/ΔCO in the DFW region was 64.0 ± 26.9 µg/m^{3}ppmv, with a range between 4.5 and 154.5 µg/m^3 ppmv. Figure 4 shows a diurnal profile of the ratio. Organic aerosol enhancement with respect to CO starts to increase in early morning after the sun rises (increased photochemical activity) and shows a decrease after sunset. The median value is variable during the overnight hours. Figure 5 shows various panels that indicate this ratio versus time color coded by the various calculated aging metrics. In considering these figures, it should be noted that these aging metrics do not estimate an absolute photochemical age but that the changes in the ratios can be used to compare photochemical processing over a certain time.

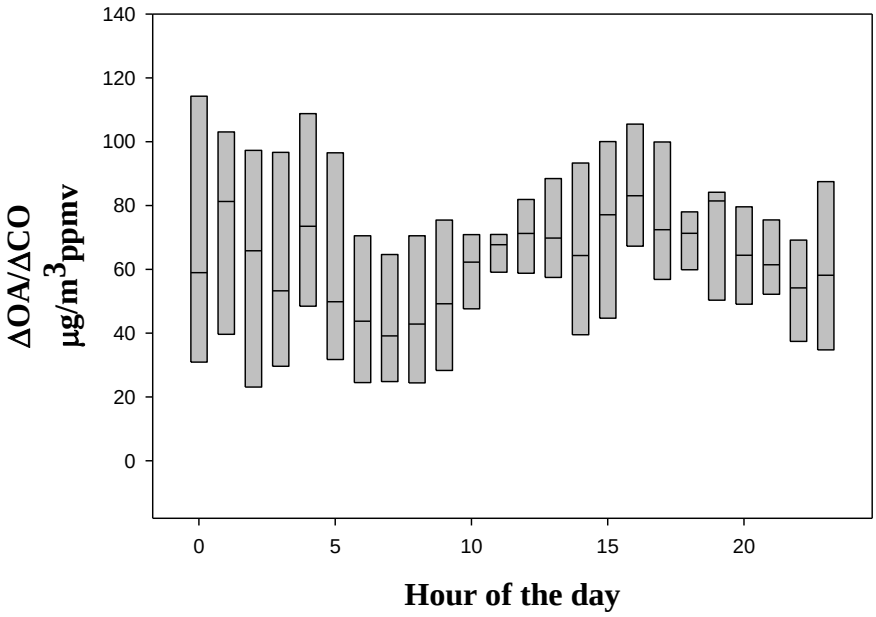

Figure 4. Diurnal profile box plots of .ΔOA/ΔCO ratio. The band in the middle shows the median, and the bottom and the top of the boxes represent the 25 and 75 percentiles.

a)

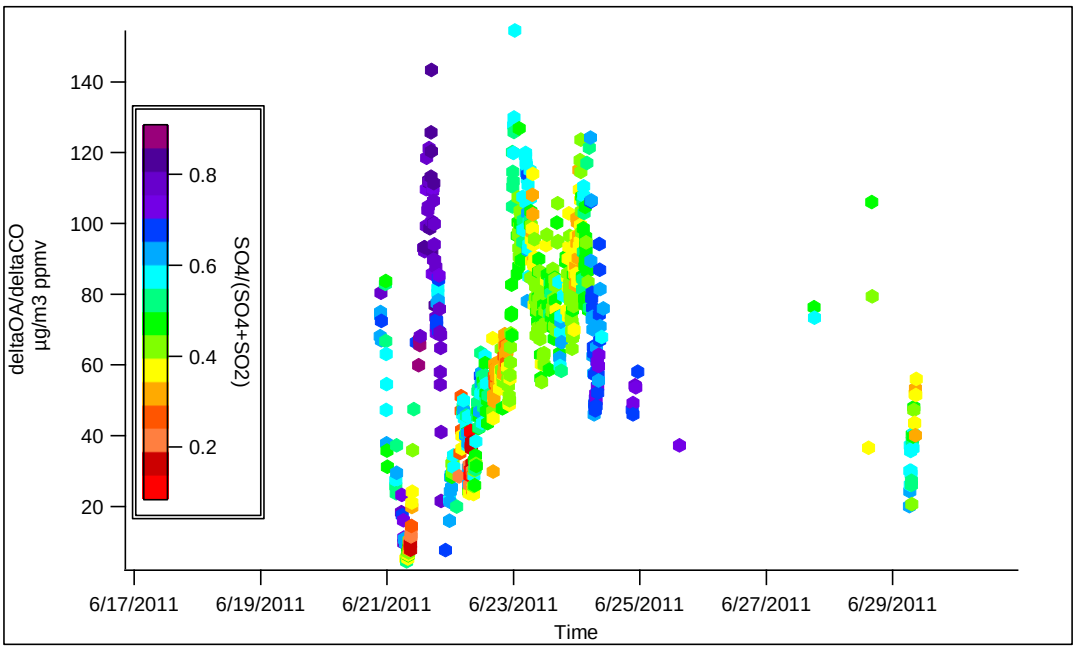

b)

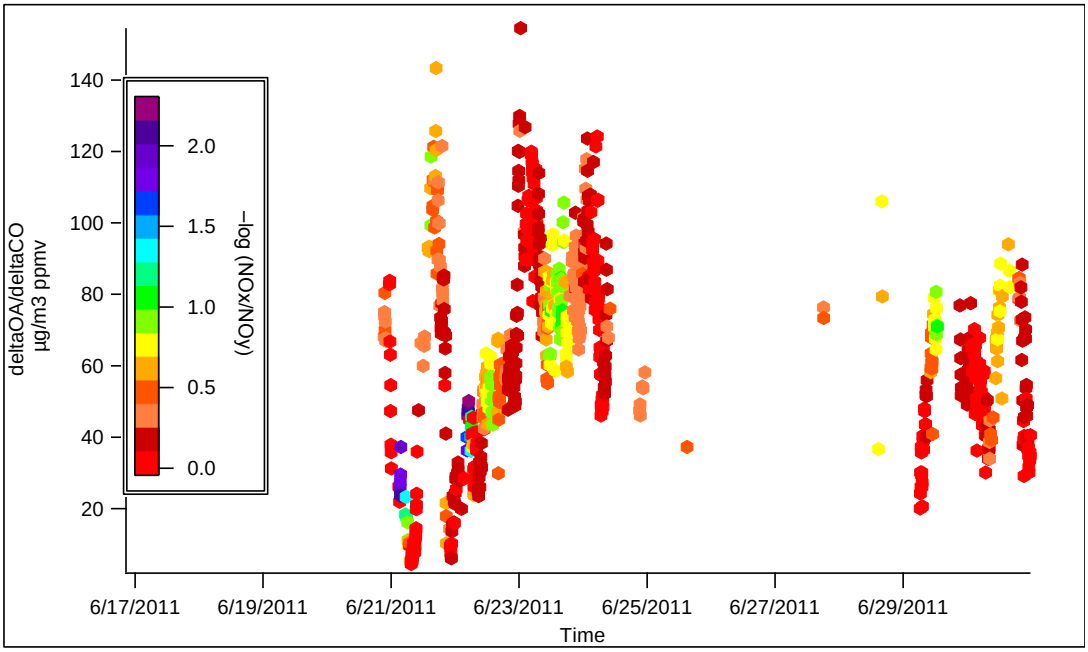
deltaOA/deltaCO
µg/m3 ppmv
140
120
100
80
60
40
20
2.0
1.5
1.0
0.5
0.0
−log (NOx/NOy)
6/17/2011
6/19/2011
6/21/2011
6/23/2011
6/25/2011
6/27/2011
6/29/2011
Time

c)

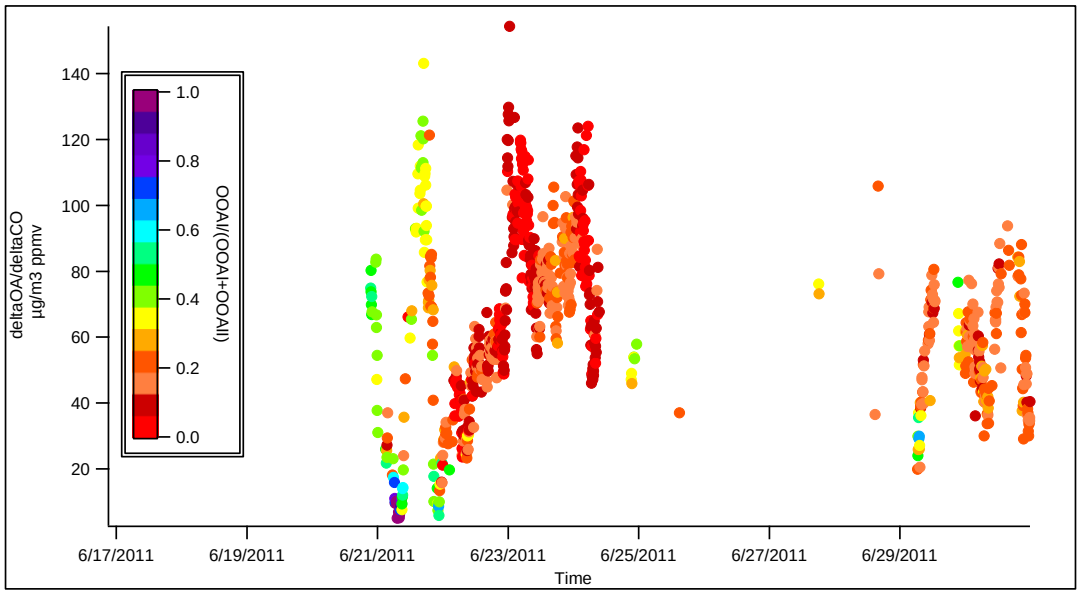
deltaOA/deltaCO
µg/m3 ppmv
140
120
100
80
60
40
20
1.0
0.8
0.6
0.4
0.2
0.0
OOAI/(OOAI+OOAII)
6/17/2011
6/19/2011
6/21/2011
6/23/2011
6/25/2011
6/27/2011
6/29/2011
Time

d)

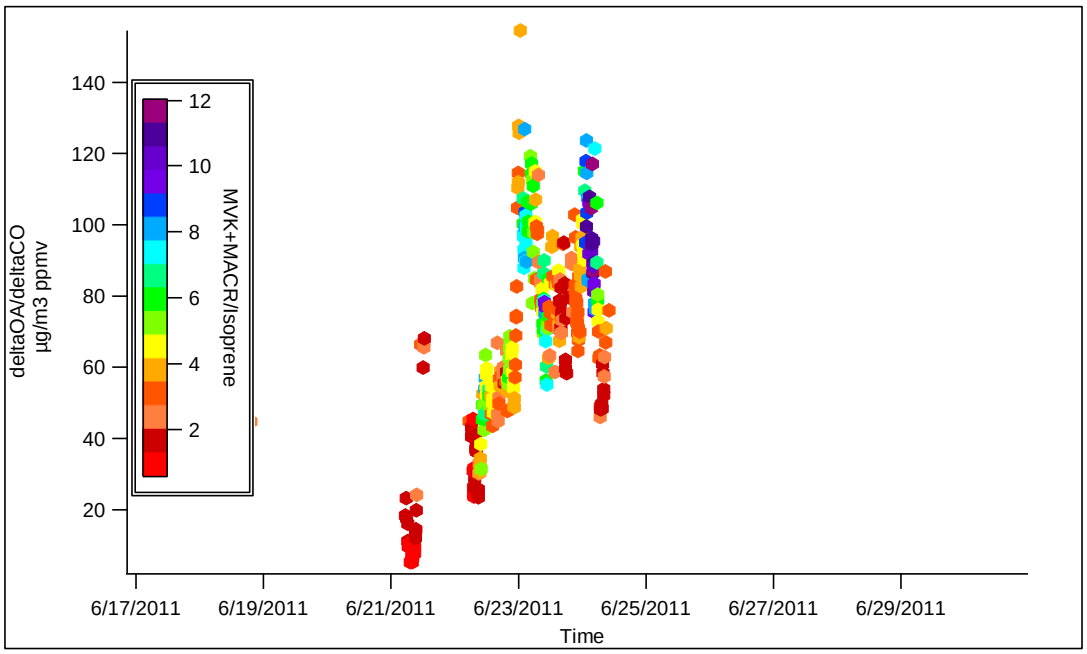

Figure 5. ΔOA/ΔCO ratios color coded by different air mass aging indicators: a.)$SO_4^{2-}/(SO_2+SO_4^{2-})$; b.) (MACR+MVK)/isoprene; c.) $-\log(NO_x/NO_y)$; d.) OOAI/(OOAI+OOAII).

Figure 5a shows the time series of ΔOA/ΔCO as a function of the sulfate aging metric. As shown in Figure 6a, there is no consistent monotonic linear relationship between the ΔOA/ΔCO values and the sulfate aging metric. Table 1 shows that the average sulfate aging metric was 0.57 ± 0.15, and Figure 5a shows that most data fall near this range, regardless of ΔOA/ΔCO. However, Figure 5a indicates a period on June 21 in the afternoon that showed enhancements in both the sulfate aging metric (approximately 0.8) and ΔOA/ΔCO (approximately 100 µg/ m^3 ppmv). The observed sulfate aging metric were greater than that measured by Hayden et al., (2011) and Hennigan et al., (2006).

Figure 5b shows the same time series but colored by the aging metric with respect to NO_x. For fresh emissions, $-\log(NO_x/NO_y) = 0$, and when 90% of NO_x is converted to NO_y., $-\log(NO_x/NO_y) = 1$ (Kleinman et al., 2008). The average metric value was 0.35 ± 0.27 (Table 1). The observed $-\log(NO_x/NO_y)$ ratios were similar to that measured by Slowik, et al., (2011) in southwestern Ontario and were smaller than the ratios measured by Kleinman et al., (2008) in New England. Similar to the sulfate aging metric, the NOx aging metric shows no consistently clear linear relationship with ΔOA/ΔCO (Figure 6b) and is enhanced during the afternoon period of June 21 (approximately 0.6).

Finally, Figure 5c indicates similar data colored by the OA aging metric. There is no consistent positive linear relationship between the ΔOA/ΔCO values and the OA aging metric (Figure 6c). However unclear, there may be an indication of a negative nonlinear pattern. The average OOAI/(OOAI+OOAII) ratio was 0.32 ± 0.23 (Table 1). Similar to the sulfate and NO_x aging metrics during the afternoon period of June 21, the OOAI/(OOAI+OOAII) values are elevated, which indicates an increased contribution of less volatile (and likely more aged) OA.

Other measured pollutants were investigated on for 21 June, and large peaks of SO_2 and NO were observed in the morning of June 21, followed by enhancement of NO_2, NOy, and sulfate in the afternoon (not shown). While ozone values were typical compared to the rest of the campaign, these findings indicate the likelihood of transport of very highly aged air.

Unfortunately, VOC data were not available during the afternoon of June 21. However, Figure 5d shows the same time series of ΔOA/ΔCO but shaded as a function of

the aging metric with respect to biogenic VOCs. Table 1 shows that the average biogenic aging metric was 2.66 ± 1.97. Ratios greater than approximately 0.54 indicate significant photochemical processing (deGouw et al., 2005; Cottrell et al., 2008). The ratios observed were significantly higher than the ratios measured by Cottrell et al., (2008). In contrast to the other aging metrics, there is a slight positive linear correlation between the biogenic aging metric values and the ΔOA/ΔCO ratios. While this may be caused by gaps in the data, it also may indicate that the OA sampled at EML represents a baseline of anthropogenic OOA with contributions of biogenic OOA beyond that.

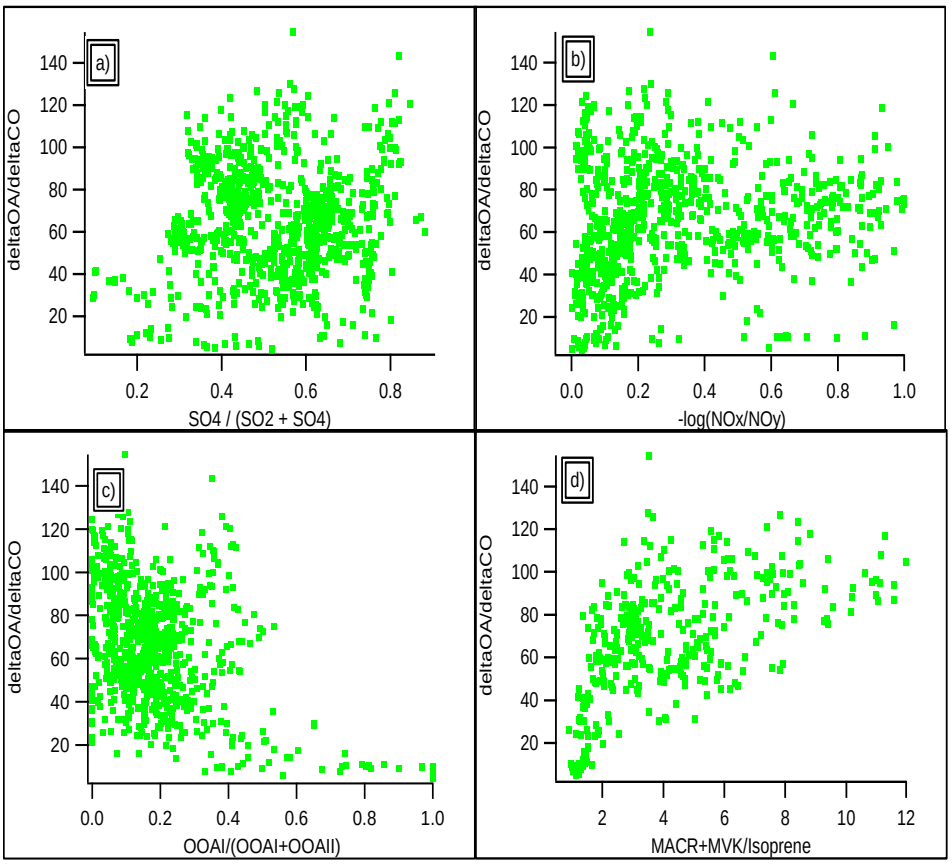

Figure 6) Relationship of age metrics and ΔOA/ΔCO a) SO_4^{2-} / (SO_2 + SO_4^{2-}) b) – log(NOx/NOy) c) OOAI(OOA I+ OOA II d) MACR+MVK/Isoprene

Table 1. Calculated mean, median, standard deviation, minimum, and maximum values of age metrics.

	$SO_4/(SO_4+SO_2)$	**OOAI/(OOAI+OOAII)**	**(MACR+MVK)/Isoprene**	**$[-\log(NO_x/NO_y)]$**
Mean	0.57	0.32	2.68	0.345
Median	0.59	0.26	1.97	0.27
S.D.	0.15	0.23	2.06	0.28
Min	0.09	6.24e-8	0.63	-0.04
Max	0.90	1	11.96	2.30

CHAPTER 4

CONCLUSIONS

Several conclusions can be made regarding the PM_1 at the EML site during the 2011 campaign. The average aerosol composition was dominated by organic matter and sulfate. Organic aerosol was correlated with anthropogenic tracers such as CO and BC which indicates a relationship between OA and combustion activities. However, the relationship between SOA processing and the biogenic aging metric indicate that it is probable that biogenic SOA forms on top of whatever is formed upwind as a result of such anthropogenic activities. OOAII dominates the total organic mass (57.4±22.9%) and correlates positively with CO (r^2 = 0.61), which indicates it is mostly dominated by relatively fresh urban SOA. The time series of ammonium and sulfate track each other indicating the predominance of ammonium sulfate relative to ammonium nitrate, whereas nitrate tracks organic matter, presumably due to similarity in volatility of locally produced aerosol. Enhancement of both $\Delta OA/\Delta CO$ and aging metrics of sulfate, NO_x and organic aerosol observed on June 21 are probably due to transport of more highly aged air to site.

Future studies on the DFW data will focus on the filter analysis. Inorganic components of aerosol collected on filters will be analyzed with IC with a focus on chloride and other inorganic components that cannot be measured with HR-ToF-AMS or that were below the detection limit of the PILS. Functional group analysis of the organic aerosol on a separate set of collected filters will allow differentiation of the relative contribution of each different functional group to water soluble organic carbon mass.

Additional HR-ToF-AMS data analyses will attempt to tease out the contribution of natural plant material to the submicron OA, which could be particularly relevant given the drought conditions experienced throughout Texas during 2011. In addition, particle number concentration and size data measured with a scanning mobility particle sizer will be studied .

Bibliography

Alfarra, M. R. *Insights into atmospheric organic aerosols using an aerosol mass spectrometer.* Machester, UK: PHD thesis, 2004.

Cottrell, Laura D., et al. "Submicron particles at Thompson Farm during ICARTT measured using aerosol mass spectrometry." *Journal Of Geophysical Research*, 2008: D08212, 18 PP.

de Gouw, J. A., et al. "Budget of organic carbon in a polluted atmosphere: Results from the New England Air Quality Study in 2002." *Journal Of Geophysical Research*, 2005: D16305, 22 PP.

de Gouw, J. A., et al. "Emission and chemistry of organic carbon in the gas and aerosol phase at a sub-urban site near Mexico City in March 2006 during the MILAGRO study." *Atmos. Chem. Phys.*, 2009: 3425–3442.

DeCarlo, P. F., et al. " Investigation of the sources and processing of organic aerosol over the Central Mexican Plateau from aircraft measurements during MILAGRO." *Atmos. Chem. Phys.*, 2010: 5257–5280.

DeCarlo, P. F., et al. "Fast airborne aerosol size and chemistry measurements above Mexico City and Central Mexico during the MILAGRO campaign." *Atmospheric Chemistry and Physics*, 2008: 4027-4048.

DeCarlo, P.F., et al. "Field-Deployable, High-Resolution, Time-of-Flight Aerosol Mass Spectrometer." *Analytical Chemistry*, 2006: 8281-8289.

Donaldson, K., and W. MacNee. "The Mechanism of Lung Injury Caused by PM10." *Issues in Environmental Science and Technology,* 1998: 21-38.

Hayden, K. L., Sills, D. M. L., Brook, J. R., Li, S.-M., Makar, P. A., Markovic, M. Z., Liu, P., Anlauf, K. G., O'Brien, J. M., Li, Q., McLaren, R. "Aircraft study of the impact of lake-breeze circulations on trace gases and particles during BAQS-Met 2007." *Atmos. Chem. Phys.*, 2011: 11, 10173-10192.

Hennigan, C. J., Sandholm, S., Saewung, K., Stickel, R. E., Huey, L.G., Weber, R. J. "Influence of Ohio River valley emissions on fine particle sulfate measured from aircraft over large regions ofthe eastern United States and Canada during INTEX-NA." *Journal Of Geophysical Research,*2006: 111, D24S04.

Hodzic, A., and J. L. Jimenez. "Modeling anthropogenically controlled secondary organic aerosols in a megacity: a simplified framework for global and climate models." *Geoscientific Model Development*, 2011: 901–917.

Hoose, C., and O. Mohler. "Heterogeneous ice nucleation on atmospheric aerosols: a review of results from laboratory experiments." *Atmos. Chem. Phys. Discuss*, 2012: 12533.

Kleinman, L. I., et al. "The time evolution of aerosol composition over the Mexico City." *Atmos. Chem. Phys.*, 2008: 1559–1575.

Kleinman, Lawrence I., et al. "Aircraft observations of aerosol composition and ageing in New England and Mid-Atlantic States during the summer 2002 New England Air

Quality Study field campaign." *Journal Of Geophysical Research*, 2007: VOL. 112, D09310.

Lanz, V.A., M.R. Alfarra, U. Baltensperger, B. Buchmann, C. Hueglin, and A.S.H. Prevot. "Source Apportionment of Submicron Organic Aerosols at an Urban Site by Factor Analytical Modelling of Aerosol Mass Spectra." *Atmospheric Chemistry and Physics*, 2007: 1503–1522.

Nemmar, A, Vanbilloen H, Hoylaerts M. F., P.H.M. Hoet, A Verbruggen, And B. Nemery. "Passage of Intratracheally Instilled Ultrafine Particles from the Lung into the Systemic Circulation in Hamster." *American Journal of Respiratory and Critical Care Medicine*, 2001: 1665-1668.

Orsini, Douglas A., Yilin Ma, Amy Sullivan, Berko Sierau, Karsten Baumann, and Rodney J. Weber. "Refinements to the particle-into-liquid sampler (PILS) for ground and airborne measurements of water soluble aerosol composition." *Atmospheric Environment* , 2003: 1243–1259.

Pope, C.A., et al. "Lung Cancer, Cardiopulmonary mortality, and long-term exposure to fine particulate air pollution." *Journal of the American Medical*, 2002: 1132-1141.

Pöschl, Ulrich. "Atmospheric Aerosols: Composition, Transformation, Climate and Health Effects." *Angewandte Chemie International Edition*, 2005: 7520-7540.

Quinn, P. K., et al. "Impact of particulate organic matter on the relative humidity dependence of light scattering: A simplified parameterization." *GEOPHYSICAL RESEARCH LETTERS*, 2005: L22809, 4 PP.

Saunders, R. W., et al. "An aerosol chamber investigation of the heterogeneous ice nucleating potential of refractory nanoparticles." *Atmospheric Chemistry and Physics*, 2010: 1227-1247.

Seinfeld, John H, and Spyros N Pandis. *Atmospheric Chemistry and Physics From Air Pollution to Climate Change.* New Jersey: John Wiley & Sons, Inc., 2006.

Slowik, J. G., et al. "Photochemical processing of organic aerosol at nearby continental sites: contrast between urban plumes and regional aerosol." *Atmos. Chem. Phys.*, 2011: 2991-3006.

Ulbrich, I.M., M.R. Canagaratna, Q. Zhang, D.R. Worsnop, and Jimenez J.L. "Interpretation of Organic Components from Positive Matrix Factorization of Aerosol Mass Spectrometric Data." *Atmospheric Chemistry and Physics* , 2009: 2891-2918.

Weber, R.J., D. Orsini, Y. Daun, Y.N. Lee, P. Klotz, and F. Brechtel. "A particle-into-liquid collector for rapid measurements of aerosol chemical composition." *Aerosol Science Technology*, 2001: 718-727.